Investigation of the Impact of the Upstream Induction Zone on LIDAR Measurement Accuracy for Wind Turbine Control Applications using Large-Eddy Simulation

Eric Simley[1], Lucy Y. Pao[1], Pieter Gebraad[2], and Matthew Churchfield[3]

[1] Department of Electrical, Computer, and Energy Engineering, University of Colorado, Boulder, CO, USA
[2] Delft Center for Systems and Control, Delft University of Technology, Delft, The Netherlands
[3] National Wind Technology Center, National Renewable Energy Laboratory, Golden, CO, USA

E-mail: eric.simley@colorado.edu

Abstract. Several sources of error exist in lidar measurements for feedforward control of wind turbines including the ability to detect only radial velocities, spatial averaging, and wind evolution. This paper investigates another potential source of error: the upstream induction zone. The induction zone can directly affect lidar measurements and presents an opportunity for further decorrelation between upstream wind and the wind that interacts with the rotor. The impact of the induction zone is investigated using the combined CFD and aeroelastic code SOWFA. Lidar measurements are simulated upstream of a 5 MW turbine rotor and the true wind disturbances are found using a wind speed estimator and turbine outputs. Lidar performance in the absence of an induction zone is determined by simulating lidar measurements and the turbine response using the aeroelastic code FAST with wind inputs taken far upstream of the original turbine location in the SOWFA wind field. Results indicate that while measurement quality strongly depends on the amount of wind evolution, the induction zone has little effect. However, the optimal lidar preview distance and circular scan radius change slightly due to the presence of the induction zone.

1. Introduction

Recently there has been great interest in feedforward control of wind turbines for rotor speed regulation and load reduction using preview measurements of the wind provided by Light Detection and Ranging (lidar) [1]-[3]. Although results suggest significant load reduction, the effectiveness of preview-based control depends on how accurately lidars can measure the wind disturbances that will interact with the rotor. Several sources of measurement error exist. Previous controller design studies have included the effects of lidar range weighting (spatial averaging of wind speeds along the lidar beam) and directional bias (errors caused by the lidar's line-of-sight not being aligned with the mean wind direction) [1, 2, 4]. Additionally, the impact of the evolution of the wind, as it travels from the measurement location to the rotor plane, on controller performance has been investigated using analytic models [3, 5]. A further source of

potential error, which has not been previously investigated, is the upstream induction zone, the region near the rotor where wind speeds slow down due to the blockage effect [6].

In this work, the impact of the induction zone on lidar measurements is investigated using the National Renewable Energy Laboratory's (NREL) Simulator fOr Wind Farm Applications (SOWFA) code [7] with the NREL 5-MW reference turbine model [8]. While many aeroelastic design codes such as NREL's FAST [9] compute the response of a turbine given a predetermined wind field, SOWFA models the two-way interaction between the wind and the turbine using large-eddy simulation (LES) coupled with FAST. This allows lidar measurements to be simulated in the presence of the induction zone. A slice of the LES wind field outside of the induction zone is used in a separate FAST simulation together with two different lidar scenarios to reveal measurement quality without induction zone effects both with and without wind evolution. Measurement quality is assessed using the coherence between the lidar measurements and the actual wind disturbances at the turbine calculated using a wind speed estimator.

The rest of the paper is organized as follows. A description of the large-eddy simulation wind field containing the wind turbine is provided in Section 2. In Section 3 the lidar measurement configuration is discussed. Section 4 describes the three scenarios used to assess lidar measurement quality and Section 5 briefly describes the wind speed estimator. A comparison of the measurement quality for the three scenarios is presented in Section 6 while Section 7 concludes the paper.

2. SOWFA Simulation

SOWFA is a coupled computational fluid dynamics (CFD) and wind turbine structural and system dynamics tool based on the OpenFOAM CFD toolbox [10] and NREL's FAST wind turbine modeling tool. It was used in this study to simulate both the turbulent atmospheric inflow and the flow about the turbine including the axial induction zone and to simulate turbine structural response in a fluid-structure coupled manner. This section describes the tool and the characteristics of the particular inflow wind used in this study.

2.1. Description of the SOWFA Simulation

SOWFA, the equations it solves, and its modeling strategies are discussed briefly here, but more details can be found in the article by Churchfield *et al.* [11]. The CFD solver component of SOWFA is typically used to perform LES, a type of CFD simulation in which the larger, energy-containing turbulent scales are directly resolved whereas the effect of the smaller scales is modeled using a subgrid-scale (SGS) model. It solves the incompressible filtered Navier-Stokes equations. The effects of atmospheric stratification are included through a buoyancy term that uses the Boussinesq buoyancy approximation. In this work, the standard Smagorinksy SGS model is used with a model constant of $C_s = 0.135$. We have found the standard Smagorinsky model allows the solver to well reproduce a logarithmic wind profile with the proper choice of model constant, vertical resolution, and grid aspect ratio following the work of Brasseur and Wei [12]. The solver uses a bottom boundary condition that applies a shear stress found using the Monin-Obukhov scaling laws, a common practice in LES of the atmospheric boundary layer.

The wind turbine aerodynamic effects are modeled using an actuator line representation of the blades. Each blade is represented as a line that rotates in time. Each line is divided into small segments, each with a center point. Velocity is sampled at the center point of each line segment and passed to FAST. The aerodynamics module of FAST uses airfoil lift and drag tables to compute the aerodynamic forces at each blade section. Those forces are passed both to the structural dynamics module of FAST and also back to the CFD solver. The CFD solver applies the computed blade forces along the actuator lines as body forces. These body forces create the axial induction zone, the rotor wake, and blade root and tip vortices. The impact of the nacelle and tower on the flow is not modeled.

The overall simulation method is to first perform a precursor LES in which the atmospheric boundary layer flow is solved upon a laterally periodic domain of uniform resolution. Because of the periodicity, a canonical horizontally homogeneous turbulent atmospheric boundary layer with its turbulence and shear develops after anywhere from 10,000 s to 40,000 s of simulation time, depending on the atmospheric stability being simulated. The typical domain size is 3–5 km in the horizontal and 0.5–2 km in the vertical with a resolution on the order of 10 m. The specific simulation investigated in this work has a domain size of 3 km $\times$ 3 km $\times$ 1 km with a resolution of 12 m. Once a well developed atmospheric boundary layer is established, then planes of inflow velocity and temperature data are sampled each time step for some duration.

These data planes are then used as inflow planes to a second simulation that contains the FAST-coupled actuator line turbines based on the NREL 5-MW reference model with rotor diameter $D = 126$ m, 90 m hub height, and rated wind speed 11.4 m/s [8]. This simulation does not use periodic boundaries. It also uses a variable-resolution mesh that has 3 m resolution around the turbines and their wakes, but the same 12 m resolution out in the undisturbed flow with a 6 m resolution zone in between. The extra resolution is necessary to capture the relevant turbulent scales that form in the turbine wakes. It is this second simulation that is used in this work to simulate lidar sampling, to sample the actual flow, and to run FAST two-way coupled with the fluid flow. All results in this paper are produced using 1000 s of data. From this point forward, a two-way coupled FAST-CFD simulation is simply referred to as a SOWFA simulation.

2.2. Large-Eddy Simulation Wind Field

The wind field used in this study was previously generated in the study by Churchfield *et al.* [11]. It is of neutral stability, meaning there are no buoyancy effects due to atmospheric stratification, and the surface roughness is 0.001 m, which is a low value typical of flow over water. The hub-height (90 m) mean wind speed and turbulence intensity are 8 m/s and 6%, respectively. Velocity contours of the mean wind field near the turbine, including the flow perturbed by the turbines are shown in Figure 1.

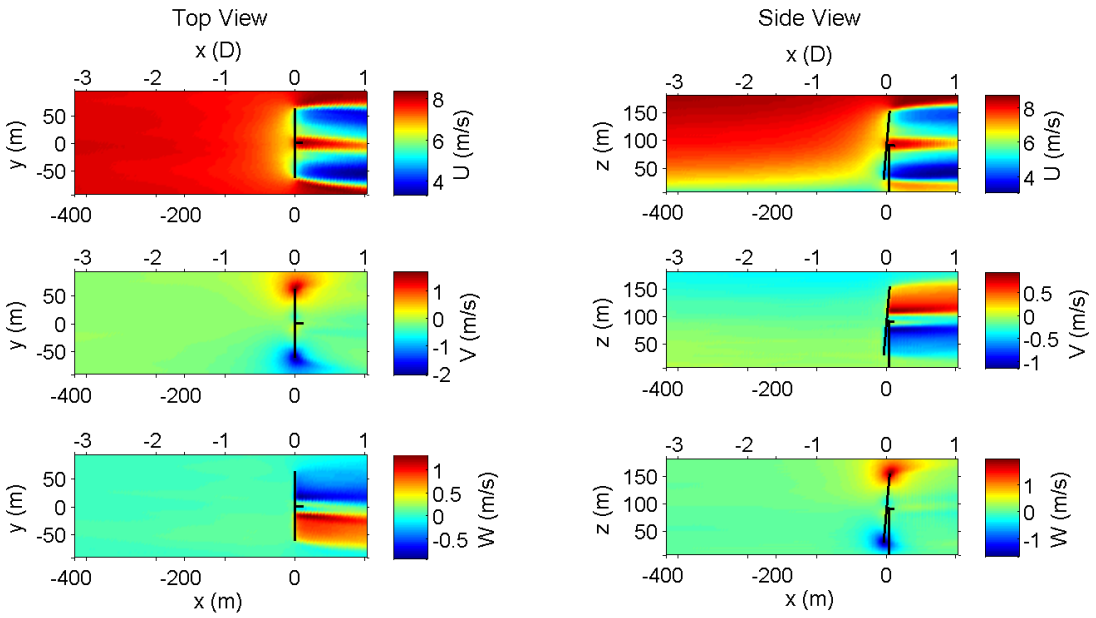

Figure 1. Mean velocities near the turbine in the SOWFA wind field. The x coordinates are expressed in meters as well as rotor diameters ($D = 126$ m).

3. Lidar Measurements

Lidar measurements are simulated using the hub-mounted lidar scenario illustrated in Figure 2, with a separate lidar corresponding to each blade. A model of the commercially available ZephIR continuous-wave (CW) lidar is used to calculate the spatial averaging inherent in lidar measurements [4]. Each lidar is focused on a scan circle with radius r and preview distance d upstream of the rotor, separated from each other by 120° in the azimuthal direction. The lidar focus points rotate around the scan circle at the same rate as the rotor.

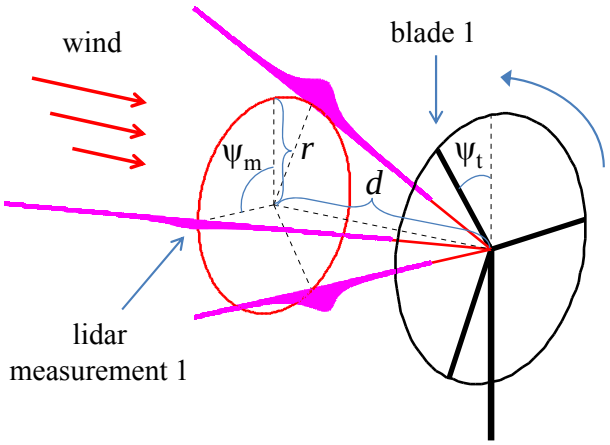

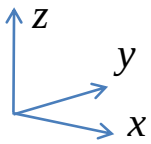

Figure 2. Lidar measurement scenario and coordinate system showing preview distance d, scan radius r, rotor azimuth angle ψ_t, and lidar measurement azimuth angle ψ_m. The lidar range weighting functions are illustrated by the magenta curves.

Because the longitudinal component of the wind speed (the x direction in Figure 2) has the greatest impact on rotor aerodynamics, an estimate of the longitudinal, or u, component of the wind is formed from lidar measurement i by dividing the range-weighted, line-of-sight measurement $u_{i,wt,LOS}$ by the x component of the lidar direction vector $\vec{\ell_i} = [\ell_{i,x}, \ell_{i,y}, \ell_{i,z}]$:

$$\hat{u}_i = -\frac{1}{\ell_{i,x}} u_{i,wt,LOS}. \tag{1}$$

The line-of-sight measurement $u_{i,wt,LOS}$ is given by integrating the dot product between the lidar direction vector and the u, v, and w wind components (corresponding to x, y, and z, respectively) along the lidar beam, weighted by the lidar's range weighting function $W(F, s)$:

$$u_{i,wt,LOS} = \int_0^\infty W(F,s) \left[-\ell_{i,x} u\left(s\vec{\ell_i}\right) - \ell_{i,y} v\left(s\vec{\ell_i}\right) - \ell_{i,z} w\left(s\vec{\ell_i}\right) \right] ds. \tag{2}$$

The peak of the range weighting function for the CW lidar is located at the focus distance F along the beam and has a full-width-half-maximum (FWHM) width that scales with the square of the focus distance. An example of the range weighting function for the ZephIR is illustrated by the magenta curves over the lidar beams in Figure 2. For the lidar parameters modeled here, the FWHM is 12.75 m when the focus distance is $F = 100$ m [4].

Rather than using estimates of the wind speeds corresponding to each individual blade as inputs to a feedforward control system, the measurements are transformed into rotor-effective quantities that can be more easily used in controller designs. Because it is assumed that the turbine has zero yaw misalignment, the rotor-effective wind disturbances of interest are the time-varying hub-height wind speed and linear horizontal and vertical shear components. Using the multiblade coordinate transformation (MBC) [13] as a function of the measurement azimuth angle ψ_m, the three lidar measurements are transformed into hub-height and shear components:

$$\begin{bmatrix} \hat{u}_{hh} \\ \hat{\Delta}_h \\ \hat{\Delta}_v \end{bmatrix} = \begin{bmatrix} \frac{1}{3} & \frac{1}{3} & \frac{1}{3} \\ -\frac{4}{3}\sin(\psi_m) & -\frac{4}{3}\sin\left(\psi_m + \frac{2\pi}{3}\right) & -\frac{4}{3}\sin\left(\psi_m + \frac{4\pi}{3}\right) \\ \frac{4}{3}\cos(\psi_m) & \frac{4}{3}\cos\left(\psi_m + \frac{2\pi}{3}\right) & \frac{4}{3}\cos\left(\psi_m + \frac{4\pi}{3}\right) \end{bmatrix} \begin{bmatrix} \hat{u}_1 \\ \hat{u}_2 \\ \hat{u}_3 \end{bmatrix}, \tag{3}$$

where $\hat{u}_{hh}$ is the hub-height, or average, wind speed and $\hat{\Delta}_h$ and $\hat{\Delta}_v$ represent the difference in wind speed across the scan circle in the horizontal and vertical directions. Finally, to adhere to the shear component definitions used in FAST, $\hat{\Delta}_h$ and $\hat{\Delta}_v$ are normalized by the hub-height component: $\hat{\delta}_h = \hat{\Delta}_h/\hat{u}_{hh}$, $\hat{\delta}_v = \hat{\Delta}_v/\hat{u}_{hh}$.

The main sources of potential lidar measurement errors can be categorized as:

- Range weighting errors caused by spatial averaging of wind speeds along the lidar beam. Some spatial averaging is beneficial, however, because the wind is also spatially filtered along the blades when aerodynamic torque and thrust are produced by the rotor.
- Directional bias errors caused by the transverse v and vertical w wind components affecting the estimate of the u component, as shown in equation 2. This error source diminishes as the scan radius decreases or the preview distance increases, which both cause the y and z components of the lidar direction vector to become smaller.
- Wind evolution errors caused by the deviation from Taylor's frozen turbulence hypothesis, which implies that wind speeds remain unchanged as they advect downstream at the mean wind speed [3, 5]. Wind evolution errors become more significant as preview distance increases, allowing more time for the measured wind speeds to change.

4. Measurement Scenarios

The aim of this work is to examine the relative impact of the induction zone on measurement quality compared to the other error sources listed in the previous section. A baseline case is created to reveal measurement quality with neither wind evolution nor induction zone effects. The second scenario introduces wind evolution errors while the third scenario adds induction zone effects. The three measurement scenarios investigated (illustrated in Figure 3) are:

- Scenario I: FAST, No Evolution. A 144 m $\times$ 144 m (1.14 D $\times$ 1.14 D) slice of wind speeds in the yz plane, at an imaginary turbine location 315 m (2.5 rotor diameters) upstream of the turbine location in SOWFA, where induction effects are negligible, is extracted from the LES wind field and used as an input to a separate FAST simulation with the NREL 5-MW turbine model using the equilibrium inflow setting [9]. The hub-height and shear wind disturbances at the turbine are estimated using turbine outputs from FAST. Lidar measurements are simulated in the original SOWFA wind field such that the lidars measure at the extracted wind field location but are located behind the imaginary rotor plane by an amount equal to the intended preview distance. This way, the proper range weighting and directional bias effects are included, but wind evolution does not occur.
- Scenario II: FAST, with Evolution. This scenario is identical to Scenario I, except that the lidar is located at the hub location of the imaginary turbine and measurements are taken at the intended preview distance upstream of the turbine. This allows the wind measured by the lidar to evolve before it reaches the location of the extracted wind field.
- Scenario III: SOWFA, with Evolution. Lidar measurements are simulated for a lidar located at the hub of the original 5-MW turbine in the SOWFA simulation. Thus the lidar measures wind that is disturbed by the rotor induction and that undergoes wind evolution. The wind disturbances at the rotor are estimated using outputs from the original turbine in SOWFA.

5. Wind Speed Estimator

The hub-height and linear shear wind disturbances that interact with the turbine are estimated using a Kalman filter described in [14] based on a linear model of the NREL 5-MW reference turbine created using FAST's linearization capabilities. Five degrees-of-freedom are included in the linear model: generator rotation, the first tower fore-aft bending mode, and the non-rotating MBC components [13] of the first flapwise blade modes. The disturbance components u_{hh},

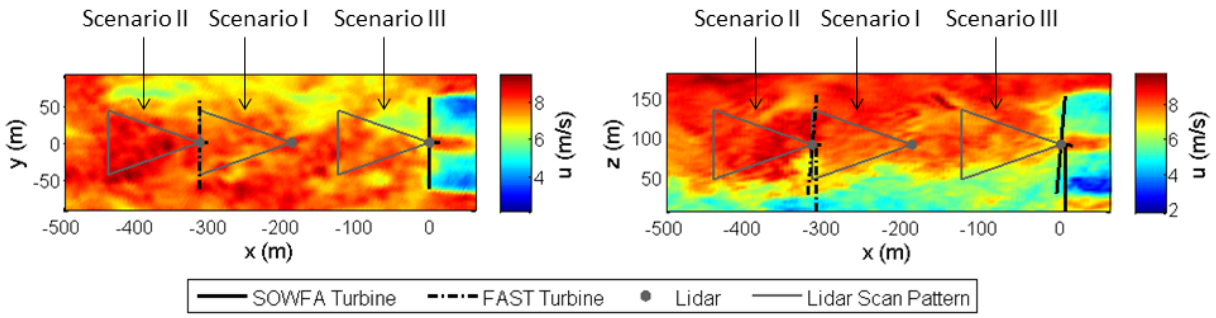

Figure 3. The three lidar measurement scenarios that are investigated.

δ_h, and δ_v are estimated using measurements of generator speed, nacelle fore-aft acceleration, and the three out-of-plane blade root bending moments. In below-rated conditions without blade pitch actuation, as in the SOWFA simulation investigated here, the resulting wind speed estimates are highly correlated with the true disturbances up to a bandwidth of 1 Hz.

Examples of the estimated wind speed disturbances and corresponding lidar measurements with scan radius $r = 0.75\ R$ (rotor radius $R = 63$ m) and preview distance $d = 0.7\ D$ for measurement scenario III are shown in Figure 4. The low hub-height component measurement is caused by the velocity deficit in the induction zone. Note the strong three-times-per-revolution ($3P$) component present in all disturbances caused by rotational sampling of the turbulence [14]. Power spectra of the estimated wind disturbances are plotted in Figure 5 for the FAST simulation used in scenarios I and II along with the SOWFA simulation from scenario III. As suggested by the time series, there is a peak in the power spectra at the $3P$ frequency 0.45 Hz as well as at the $6P$ frequency 0.91 Hz due to rotational sampling of the turbulence by the blades. Because the linear model used in the Kalman filter estimator does not account for dynamic inflow [9], the magnitude of the wind fluctuations in the SOWFA simulation is underestimated slightly.

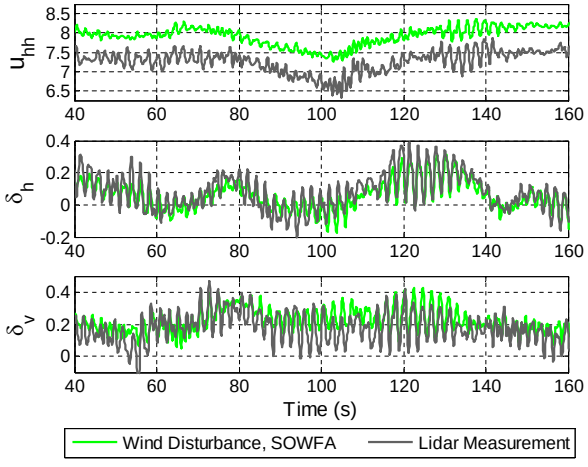

Figure 4. Estimated and measured hub-height and shear components, low-pass filtered with a cutoff frequency of 1 Hz, for measurement scenario III using a scan radius $r = 0.75\ R$ and preview distance $d = 0.7\ D$.

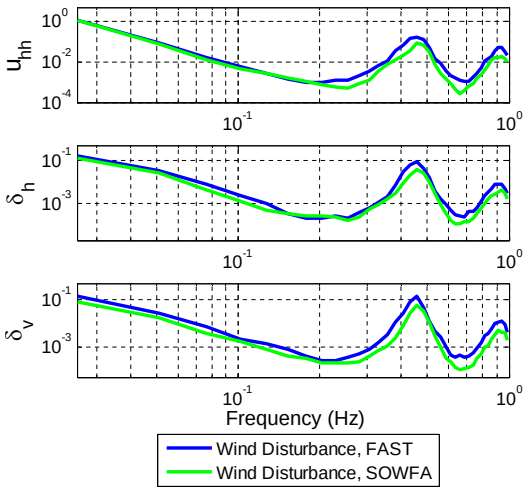

Figure 5. Power spectral densities of the estimated hub-height and shear wind disturbances for the FAST and SOWFA turbine simulations.

6. Measurement Simulation Results

Measurement quality is determined by computing the coherence between the lidar measurements and the estimated disturbances at the turbine. Coherence describes the correlation between two signals as a function of frequency, taking on values between 0 and 1, with 1 indicating perfect correlation [15]. Measurement quality for the three wind components is assessed for the three different scenarios using a variety of lidar scan radii r and preview distances d. The measurement azimuth angle (shown in Figure 2) is determined so that each lidar measures the wind that will reach its corresponding blade, using the formula: $\psi_m = \psi_t + \omega_t \cdot (d/U_{hh} + t_{offset})$, where ω_t is the rotational rate of the rotor in radians/s, U_{hh} is the mean hub-height wind speed, and t_{offset} is a tuning parameter that is used to correct for the arrival time of the wind potentially differing from d/U_{hh}. In the results presented here, optimal values of t_{offset} are found for each combination of scan radius and preview distance investigated. Note that the achievable measurement coherence depends on the specific lidar scan scenario. Therefore, the results presented here cannot necessarily be extended to other lidar configurations.

6.1. Optimal Measurement Parameters for Individual Wind Components

When optimizing the measurement quality of the three individual wind components, the chosen objective is to minimize the mean square error (MSE) between the lidar measurements and the wind disturbances that arrive at the turbine. As explained in [15], the minimum achievable MSE after properly filtering a lidar measurement to form an estimate $\hat{w}_t$ of the true disturbance w_t, can be defined in the frequency domain as:

$$\overline{(w_t - \hat{w}_t)^2} = \int_0^{f_{max}} S_{tt}(f) \left(1 - \gamma_{tm}^2(f)\right) df, \tag{4}$$

where $S_{tt}(f)$ is the power spectrum of the wind disturbance, $\gamma_{tm}^2(f)$ is the coherence between the lidar measurements and the true disturbance, and f_{max} is the imposed bandwidth of the MSE calculation. The value f_{max} is chosen to be 1 Hz because the wind speed estimator is only reliable up to this frequency and, for the NREL 5-MW reference model, the bandwidth of the blade pitch actuators, which would be used in a lidar-based control system for load reduction, is approximately 1 Hz [1, 2]. Minimizing the MSE expression in equation 4 over all scan radii r and preview distances d is equivalent to maximizing the objective function:

$$J(r, d) = \int_0^{f_{max}} S_{tt}(f)\gamma_{tm}^2(f) df. \tag{5}$$

Knowledge of the mean velocity deficits in the induction zone can be used to estimate the equivalent freestream velocities based on the lidar measurements. But the corrections do not affect measurement coherence, and thus do not reduce MSE when optimal filtering is employed.

So that the results of scenario III can be fairly compared with scenarios I and II, the wind disturbance power spectra from the FAST simulation, which are expected to be more accurate due to the lack of dynamic inflow, are used for $S_{tt}(f)$ when calculating $J(r, d)$ in all scenarios. Figure 6 shows this objective function plotted against r and d for the three wind disturbance components and three measurement scenarios, normalized by the maximum value for each case.

Table 1 displays the optimal scan radii and preview distances corresponding to the maxima in Figure 6, i.e., the parameters that minimize the MSE of the wind measurements for all components and scenarios. Additionally, Table 1 lists the normalized objective functions that are achieved by these r and d. The objective integrals are normalized by the measurement quality of scenario I as well as normalized by the integrals that would occur if measurement coherence were 1 at all frequencies. The first normalization allows scenarios II and III to be compared to the baseline case without wind evolution and induction zone effects. The latter normalization describes how close all scenarios are to representing perfect measurements.

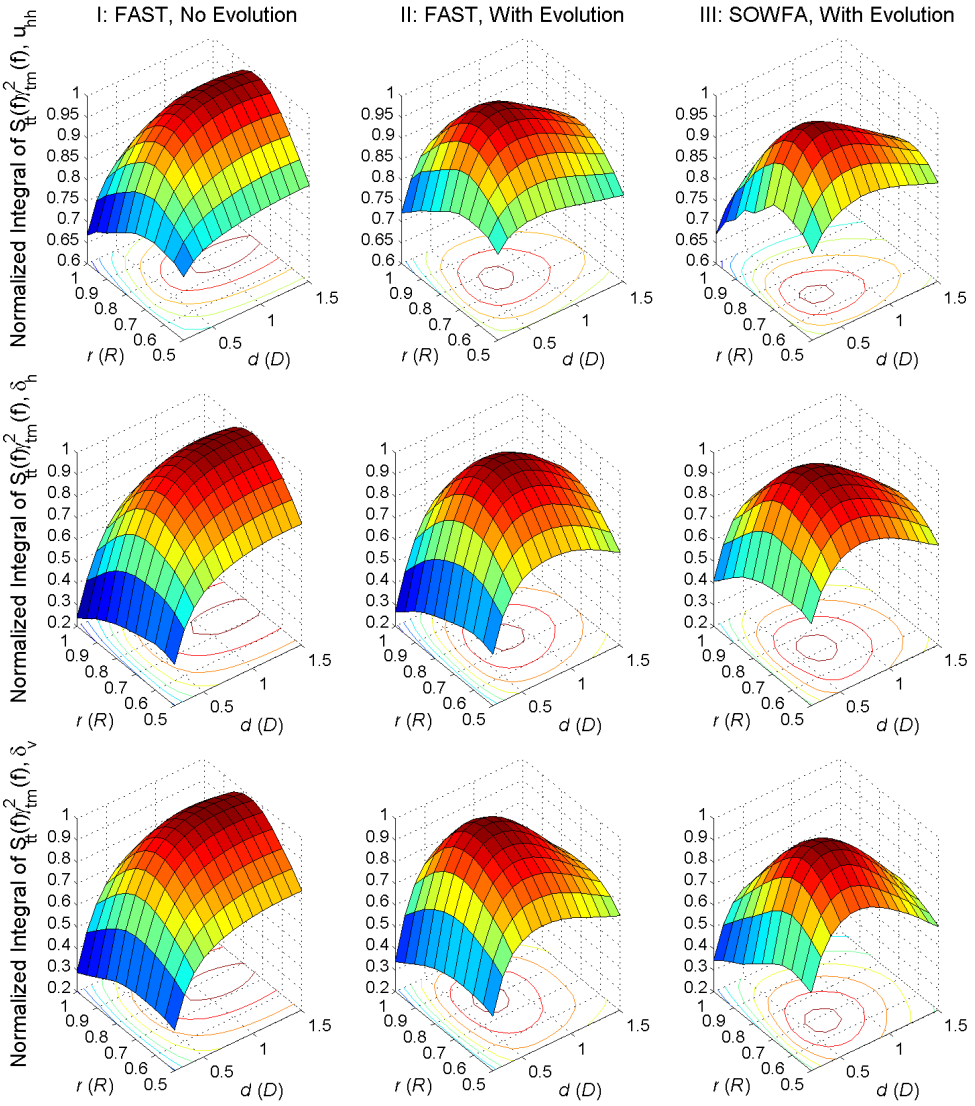

Figure 6. Measurement quality as a function of r (in rotor radii R) and d (in rotor diameters D) for all three disturbances (rows) and all measurement scenarios (columns).

Table 1. Optimal scan radii (in units of rotor radii R), preview distances (in units of rotor diameters D), and measurement quality integrals normalized by their values in scenario I as well as by their values assuming perfect measurement coherence (in parentheses).

	r (R)			d (D)			Measurement Quality		
Scenario	u_{hh}	δ_h	δ_v	u_{hh}	δ_h	δ_v	u_{hh}	δ_h	δ_v
I	0.75	0.75	0.75	1.1	1.2	1.2	1.00 (0.91)	1.00 (0.87)	1.00 (0.84)
II	0.75	0.75	0.80	0.7	0.8	0.7	0.93 (0.85)	0.89 (0.77)	0.86 (0.72)
III	0.70	0.70	0.70	0.6	0.7	0.7	0.95 (0.86)	0.91 (0.79)	0.88 (0.74)

6.2. Discussion of Results

Figure 6 and Table 1 reveal that lidar scan radii between 70% and 80% blade span yield the best measurement correlation. Lidar measurements at these scan radii, where aerodynamic torque production by the blades is the highest, are most representative of the rotor-effective wind disturbances. For scenario I, the optimal preview distances are between 1.1 and 1.2 rotor diameters. Shorter preview distances suffer from directional bias errors because of large measurement angles. But greater preview distances cause the lidar probe volumes to become too large, resulting in excessive spatial averaging [4]. As shown in Table 1, when wind evolution is introduced to the measurement simulations, the optimal preview distances are reduced to between 0.7 and 0.8 rotor diameters (Scenario II) and between 0.6 and 0.7 rotor diameters (Scenario III). The wind evolves more over greater distances, so measurements closer to the turbine, while producing larger directional bias errors, are overall more correlated with the true disturbances. In addition, greater preview distances exaggerate errors caused by wind shear (wind speeds measured at different heights reach the turbine at different times) and uncertainty in the rotor azimuth angle when the wind arrives at the turbine due to variable rotor speed.

As revealed in Table 1, measurement correlation is higher for the hub-height component than for the shear components in all three cases. This is likely due to the transverse v and vertical w components corrupting the shear measurements more than the hub-height component measurements, where they are averaged out more. Figure 7 shows the measurement coherence curves corresponding to the optimal scan radii and preview distances for all scenarios. When wind evolution is introduced to the simulations (Scenario II), measurement correlation decreases by 7–14%. This is most evident at the peaks around the 3P and 6P frequencies. However, when induction zone effects are included, measurement correlation increases slightly. This improvement is largely due to the increased measurement coherence around 0.1 Hz in all components. For comparison, measurement coherence curves for scenario III using the optimal scan parameters from scenario II, without the induction zone, are also plotted in Figure 7.

It is difficult to determine exactly what causes the slight improvement to measurement quality in Scenario III. It was found that the upstream turbulence intensity is only affected by the rotor when less than a quarter of a rotor diameter upstream of the turbine. Therefore, it is unlikely that any decrease in turbulence improves measurement quality. However, Figure 1 shows that as the wind approaches the rotor, it is deflected out toward the edge of the rotor disc. So in order to measure the wind that reaches the rotor at 75% to 80% blade span, which is optimal for Scenario II, the lidar should actually be focused at slightly smaller scan radii. The smaller scan radii allow for shorter preview distances, while only slightly increasing the measurement angles,

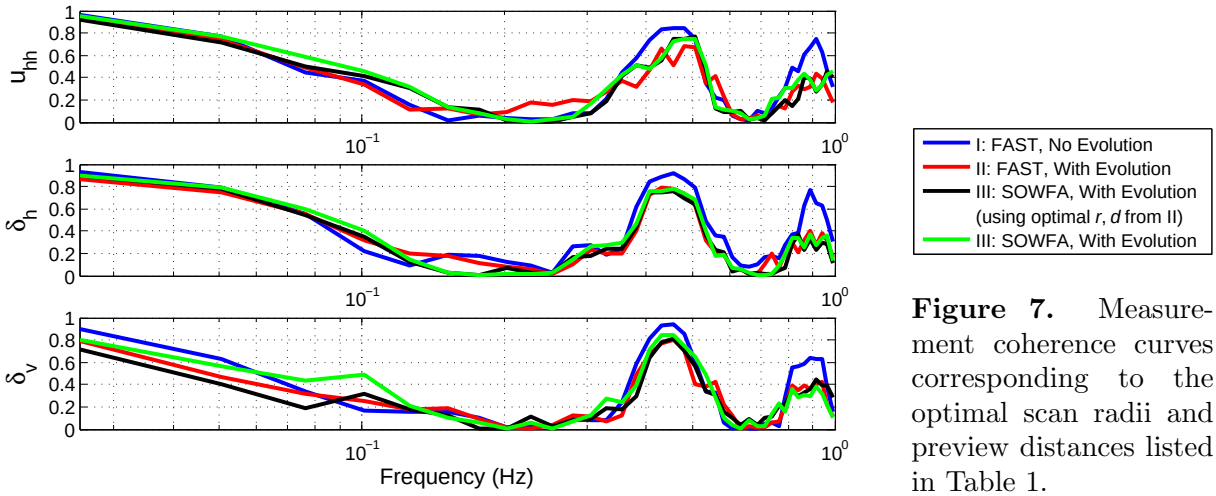

Figure 7. Measurement coherence curves corresponding to the optimal scan radii and preview distances listed in Table 1.

and thus not increasing directional bias errors by much. The shorter preview distances, in turn, result in less wind evolution which likely accounts for the higher measurement coherence.

7. Conclusions

Results from the three lidar scenarios investigated suggest that wind evolution is a significant source of error while the induction zone, rather than acting as a further error source, allows marginally better measurement coherence with slightly different optimal lidar scan parameters. However, only a 1000 s period of data was analyzed, and more simulation results should be obtained before concluding that the presence of the induction zone indeed significantly improves measurement performance. Furthermore, the results presented here were obtained using simulations with perfect yaw alignment, knowledge of the true arrival time of the wind, and the assumption that the measurement correlation statistics, necessary to calculate the optimal filter, were known *a priori*. In reality, with time-varying wind conditions, such an ideal measurement scenario is difficult to obtain; further work is necessary to evaluate lidar measurements in more realistic conditions. Simulations using different wind conditions should also be investigated to determine how measurement coherence is affected by stability, mean wind speed, and turbulence intensity. Finally, a more practical objective function should be introduced to find the single set of scan parameters that minimizes the combined impact of all three wind disturbances on turbine loads when using feedforward control.

Acknowledgments

This work was supported by the US National Renewable Energy Laboratory as well as by a Fulbright US Student Program fellowship for research in Denmark.

References

[1] Dunne F, Schlipf D, Pao LY, Wright AD, Jonkman B, Kelley N and Simley E 2012 Comparison of two independent LIDAR-based pitch control designs *Proc. AIAA Aerospace Sciences Meeting* (Nashville, TN)
[2] Schlipf D, Schlipf DJ and Kühn M 2013 Nonlinear model predictive control of wind turbines using LIDAR *Wind Energy* **16** 7
[3] Laks J, Simley E and Pao LY 2013 A spectral model for evaluating the effect of wind evolution on wind turbine preview control *Proc. American Control Conference* (Washington, D.C.)
[4] Simley E, Pao LY, Frehlich R, Jonkman B and Kelley N 2014 Analysis of light detection and ranging wind speed measurements for wind turbine control *Wind Energy* **17** 3
[5] Bossanyi EA 2012 Un-freezing the turbulence: Improved wind field modeling for investigating lidar-assisted wind turbine control. *Proc. European Wind Energy Association Annual Event* (Copenhagen, Denmark)
[6] Medici D, Ivanell S, Dahlberg J-Å and Alfredsson PH 2011 The upstream flow of a wind turbine: blockage effect *Wind Energy* **14** 5
[7] Churchfield M and Lee S 2012 NWTC design codes (SOWFA) *http://wind.nrel.gov/designcodes/simulators/SOWFA/*
[8] Jonkman J, Butterfield S, Musial W and Scott G 2009 Definition of a 5-MW reference wind turbine for offshore system development *Tech. Rep. 500-38060* National Renewable Energy Laboratory, Golden, CO
[9] Jonkman J and Buhl M 2005 FAST user's guide *Tech. Rep. 500-38230* National Renewable Energy Laboratory, Golden, CO
[10] OpenCFD 2010 OpenFOAM The open source CFD toolbox, user's manual, version 1.7.1 Reading, UK
[11] Churchfield MJ, Lee S, Michalakes J and Moriarty PJ 2012 A numerical study of the effects of atmospheric and wake turbulence on wind turbine dynamics *J. Turbulence* **13** 14
[12] Brasseur JG and Wei T 2010 Designing large-eddy simulation of the turbulent boundary layer to capture law-of-the-wall scaling *Phys. Fluids* **22** 2
[13] Bir G 2008 Multiblade coordinate transformation and its application to wind turbine analysis *Proc. AIAA Aerospace Sciences Meeting* (Reno, NV)
[14] Simley E and Pao LY 2013 Design and evaluation of a wind speed estimator for hub-height and shear components *Proc. European Academy of Wind Energy PhD Seminar* (Visby, Sweden)
[15] Simley E and Pao LY 2013 Reducing LIDAR wind speed measurement error with optimal filtering *Proc. American Control Conference* (Washington, D.C.)